JOURNAL OF NEUROTRAUMA 31:1–9 (XXXX 00, 2014)

DOI: 10.1089/neu.2013.3319

Original Article

Very High Resolution Ultrasound Imaging for Real-Time Quantitative Visualization of Vascular Disruption after Spinal Cord Injury

Marc Soubeyrand,[1] Anna Badner,[1,3] Reaz Vawda,[1] Young Sun Chung,[1] and Michael G. Fehlings[1–3]

Abstract

Spinal cord injury (SCI) is characterized by vascular disruption with intramedullary hemorrhage, alterations in blood-spinal cord barrier integrity, and perilesional ischemia. A safe and easily applied imaging technique to quantify evolving intraspinal vascular changes after SCI is lacking. We evaluated the utility of very high resolution ultrasound (VHRUS) imaging to assess SCI-induced vascular disruption in a clinically relevant rodent model. The spinal cords of Wistar rats were lesioned at the 11th thoracic vertebra (Th11) by a 35 g 1-minute clip compression. Three-dimensional quantification of intraspinal hemorrhage using VHRUS (at an acute 90-min and subacute 24-h time point post-SCI) was compared with lesional hemoglobin and extravasated Evans blue dye measured spectrophotometrically. The anatomy of hemorrhage was comparatively assessed using VHRUS and histology. Time-lapse videos demonstrated the evolution of parenchymal hemorrhage. VHRUS accurately depicted the structural (gray and white matter) and vascular anatomy of the spinal cord (after laminectomy) and was safely repeated in the same animal. After SCI, a hyperechoic signal extended from the lesion epicenter. Significant correlations were found between VHRUS signal and hemorrhage in the acute ($r = 0.88$, $p < 0.0001$) and subacute ($r = 0.85$, $p < 0.0001$) phases and extravasated Evans blue (a measure of vascular disruption) in the subacute phase ($r = 0.94$, $p < 0.0001$). Time-lapse videos demonstrated that the expanding parenchymal hemorrhage is preceded by new perilesional hemorrhagic foci. VHRUS enables real-time quantitative live anatomical imaging of acute and subacute vascular disruption after SCI in rats. This technique has important scientific and clinical translational applications.

Key words: blood spinal cord barrier; echography; hemorrhage; spinal cord injury; ultrasound

Introduction

Traumatic spinal cord injury (SCI) is a devastating condition leading to impairment in motor, sensory, and autonomic functions, and available therapeutic options for patients remain limited.[1–4] SCI induces the mechanical destruction of the blood vessels, thereby generating a parenchymal hemorrhage (PH), which contributes to the primary injury.[5] Subsequently, the vascular damage continues to extend along the rostrocaudal axis of the spinal cord because of progressive ischemia, vasospasm, and disruption of the blood spinal cord barrier (BSCB). This constitutes the secondary injury [6] and leads to the abnormal passage of blood-borne species ranging from small molecules (including albumin) to inflammatory cells and erythrocytes (hence PH) into the parenchymal intercellular space. The BSCB disruption can persist for up to 1 month with a maximum at about 24 h post-SCI.[7–9]

Techniques available to assess vascular disruption in pre-clinical studies can be classified as either imaging or nonimaging techniques. The standard nonimaging techniques involve spectrophotometric quantification of the amount of hemoglobin (using Drabkin reagent on homogenized samples of lesioned spinal cord) and dyes such as Evans blue (after pre-sacrificial intravenous injection) extravasated in the spinal cord parenchyma.[10,11] The standard imaging techniques include magnetic resonance imaging (MRI),[12] quantitative autoradiography,[8] and immunohistology.[13,14] While noninvasive, MRI requires expensive infrastructure and generates relatively low resolution images. Histologically based methods are limited to one time point of assessment, and necessitate animal sacrifice. Hence, there is a clear need for a safe high resolution technique to assess the vascular disruption after SCI that can be applied serially and in real time without compromising the spinal cord or necessitating animal sacrifice.

[1]Division of Genetics and Development, Toronto Western Research Institute, Krembil Neuroscience Program, University Health Network, Toronto, Ontario, Canada.
[2]Division of Neurosurgery and Spinal Program, University of Toronto, Toronto, Ontario, Canada.
[3]Institute of Medical Science, Faculty of Medicine, University of Toronto, Toronto, Ontario, Canada.

Various studies in clinical and experimental settings have shown that ultrasound (US) imaging can be used to visualize the PH subsequent to SCI.[15–21] In experimental studies, the highest frequencies used were 10–12 MHz,[18–21] but the small diameter of the rat spinal cord (3–4 mm) limited the resolution of imaging. More recent US devices using very high frequencies (40–55 MHz) have been specifically designed to image small animals with spatial resolutions as low as 30 microns per pixel.[22,23] To our knowledge, very high resolution US (VHRUS) has never been used for imaging the anatomical and vascular changes after experimental contusion-compression SCI in live rodents.

We have therefore developed a protocol to image the rat spinal cord with VHRUS, and the present study was performed to achieve the following three objectives: (1) to characterize the anatomical features of the intact spinal cord; (2) to characterize and quantify the vascular changes in the spinal cord during the acute and subacute phases of SCI (respectively defined as 90 min and 24 h post-SCI in our study) ; and (3) to validate VHRUS readings against several other techniques including histology and spectrophotometric analysis of hemorrhage (using Drabkin reagent) and vascular permeability (using Evans blue dye).

Methods

The protocols used in the present study were approved by the animal ethics board (AUP979) of the University of Health Network, Toronto, Canada. The study design is summarized in Figure 1.

Surgical preparation and SCI model

Female Wistar rats weighing approximately 250–300 g were anesthetized with 2% isoflurane and placed on a platform (Vevo imaging station, Visualsonics, Toronto, Canada) with a custom-made animal stabilization frame (Fig. 2). The incisor teeth were used to secure the rat into a nose cone attached to the frame and connected to the anesthesia system. A laminectomy was performed from the 10th thoracic (Th10) vertebra to Th12. The tips of a hemostatic forceps connected to the frame were bent to fit the transverse processes of Th13. Once Th13 was clamped, the spine was slightly tightened and lifted up from the platform, and then stabilized by locking the frame. Stabilization prevented spinal cord movements induced by the animal's respiration without affecting breathing. Spinal cord injury was performed at Th11 using a 35 g custom-modified aneurysm clip, and compression was maintained for 60 sec.[24,25]

US imaging

Ultrasound gel (Ultrasound Scanning Gel, Medi-Inn, Canada) was applied on the dorsal aspect of the dura mater. The VHRUS probe (44 MHz, Vevo 770, Visualsonics, Toronto, Canada) was attached to the rail mount of the Vevo Integrated Rail system III (Visualsonics, Toronto, Canada) by an integrated clamp. At the junction between the clamp and the rail, the motor stage allowed three-dimensional (3D) acquisitions. The rail mount was then pulled down until the distance between the acoustic window (top of the real-time image) and the middle of the spinal cord (identified by the central canal) was 6 mm (the focal length of the transducer). The scanhead was rotated and tilted to obtain a strict sagittal view and its position was locked. VHRUS acquisitions were made either in B-mode or in power Doppler mode. For each mode, two-dimensional (2D) and 3D acquisitions were performed.

To perform 3D acquisitions, the 3D motor stage traveled a distance of 6 mm in a series of steps from the left to the right of the spinal cord. At each step, the scanhead took a 2D image (i.e. slice), and the distance between each slice was 102 μm. Each slice was

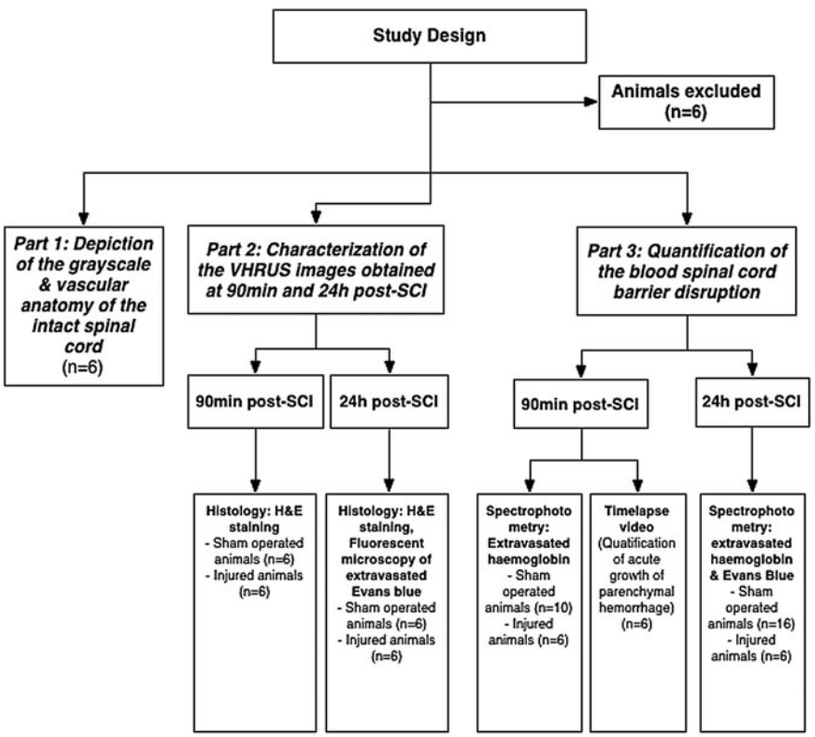

FIG. 1. Flowchart of the study design. Six animals with an intraspinal hyperechoic signal detectable by VHRUS immediately after laminectomy were excluded from the study. VHRUS, very high resolution ultrasound; SCI, spinal cord injury.

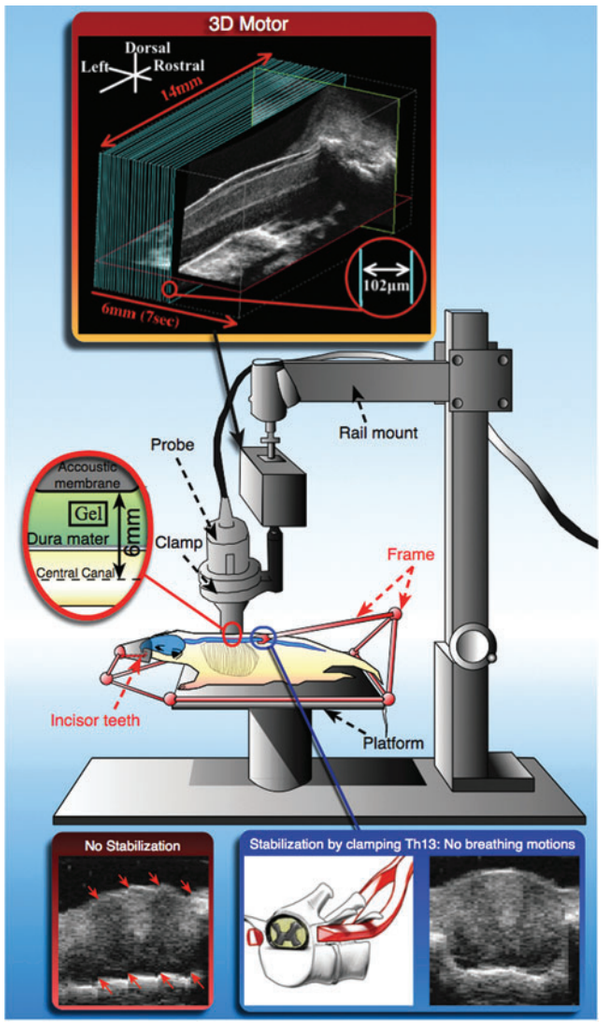

4C ▶

FIG. 2. Experimental approach and ultrasound platform schematic. If the spine is not stabilized, the respiratory motions generate distortions in the reconstructed axial slice (red arrows). With stabilization, the respiratory artifacts are no longer observed.

stacked and assembled together to form a 3D file. Each 3D acquisition took 7 sec in B-mode and 4 min in power Doppler mode.

Histology

Animals were anesthetized terminally with an overdose of inhalation isoflurane and perfused intracardially with 60 mL phosphate buffered saline 5 times, then with 60 mL 4% paraformaldehyde (PFA) once. The spinal cord was isolated, placed in 4% PFA for tissue fixation and then in 30% sucrose at 4°C overnight. The spinal cord was then embedded in OCT™ (Tissue-Tek,® Sakura,® Torrance, CA) and sagittal cryosections 20 microns thick were obtained and placed on slides for histological analysis stained using hematoxylin and eosin (HE).

In the animals kept alive for imaging at 24 h, the extent of BSCB disruption was examined by injecting 2% Evans blue dye through the femoral vein 30 min before sacrificial perfusion. Evans blue binds to albumin and can only extravasate across a disrupted BSCB. It autofluoresces and in the case of BSCB disruption, its extravasation can be directly imaged with a fluorescent microscope (DMR8, Leica, Solms, Germany).

Part 1. Structural and vascular anatomy of the intact spinal cord

In six sham-operated animals, two 3D acquisitions were successively performed in B-mode and power Doppler mode before harvesting the spinal cords for histologic evaluation. These 3D files were subsequently processed with Osirix software (Pixmeo, Geneva, Switzerland) to obtain multiplanar reconstructions (MPR) that describe the structural (gray and white matter) and vascular anatomy of the intact spinal cord.

Part 2. Characterization of post-SCI changes observed with VHRUS

Two sets of 12 animals each (6 injured, 6 sham-operated) were used to characterize the images obtained at the acute (90 min) and subacute (24 h) phases. For each animal, the spinal cord was harvested for histological analysis to characterize the tissue changes detected by VHRUS.

Part 3. Quantification of PH and BSCB disruption with VHRUS

Two sets of 22 rats each ($n = 16$ injured rats, 6 sham-operated) were used to assess PH in the acute phase (90 min) with VHRUS as well as with Drabkin reagent. The extent of BSCB disruption in the subacute phase (24 h) was measured by examining vascular permeability, which is correlated with the amount of extravasated parenchymal Evans blue.[26]

Spectrophotometric quantification of PH. After 24 h post-SCI, Evans blue was injected through the femoral vein 30 min before sacrificial perfusion. A 1-cm segment of spinal cord centered on T11 (the lesion epicenter) was isolated, crushed into powder, sonicated, weighed, and split into two equal samples—one to quantify the amount of extravasated hemoglobin (PH) using Drabkin assay and the other to quantify the amount of extravasated Evans blue by spectrophotometry (Wallac 1420 VICTOR2™ Perkin Elmer, Waltham, MA) as described previously.[27–30]

VHRUS quantification of PH. The 3D files were analyzed with ImageJ software. First, the contrast was set to maximum so that each pixel whose value was inferior to ''127'' became black (i.e., ''0'') whereas the other ones became white (i.e., ''255''). The analysis was then performed on a stack of 15 sagittal slices centered on the midline. On each slice, a 10-mm long region of interest (ROI) corresponding to a complete segment of spinal cord was delineated, and the software calculated the sum of values of all pixels belonging to the ROI (''VHRUS-Slice-Score''). All the VHRUS-Slice-Scores were added together to obtain the ''VHRUS-Global-Score.'' Each VHRUS-Global-Score was measured by three independent observers to determine the interobserver variability and twice by one observer to determine the intraobserver variability.

Statistical analysis. Statistical analyses were performed with Graphpad Prism software (La Jolla, CA). To determine whether a correlation existed between the values obtained by spectrophotometry and the VHRUS-Global-Score, the Pearson correlation coefficient was calculated. The intraobserver and interobserver variabilities in measuring the VHRUS-Global-Scores were similarly assessed by calculating the Pearson correlation coefficient.

Time-lapse VHRUS video recording. To characterize the development of the PH, a time-lapse video was generated by acquiring a midline slice every minute. The first slice was acquired at 2 min post-SCI, and the VHRUS-Slice-Score was calculated at 2 (used as the baseline), 4, 6, 8, 10, 12, 15, 20, 25, 30, 40, 50, 60, 70, 80, and 90 min post-SCI. Each VHRUS-Slice-Score was expressed as a percentage of the baseline.

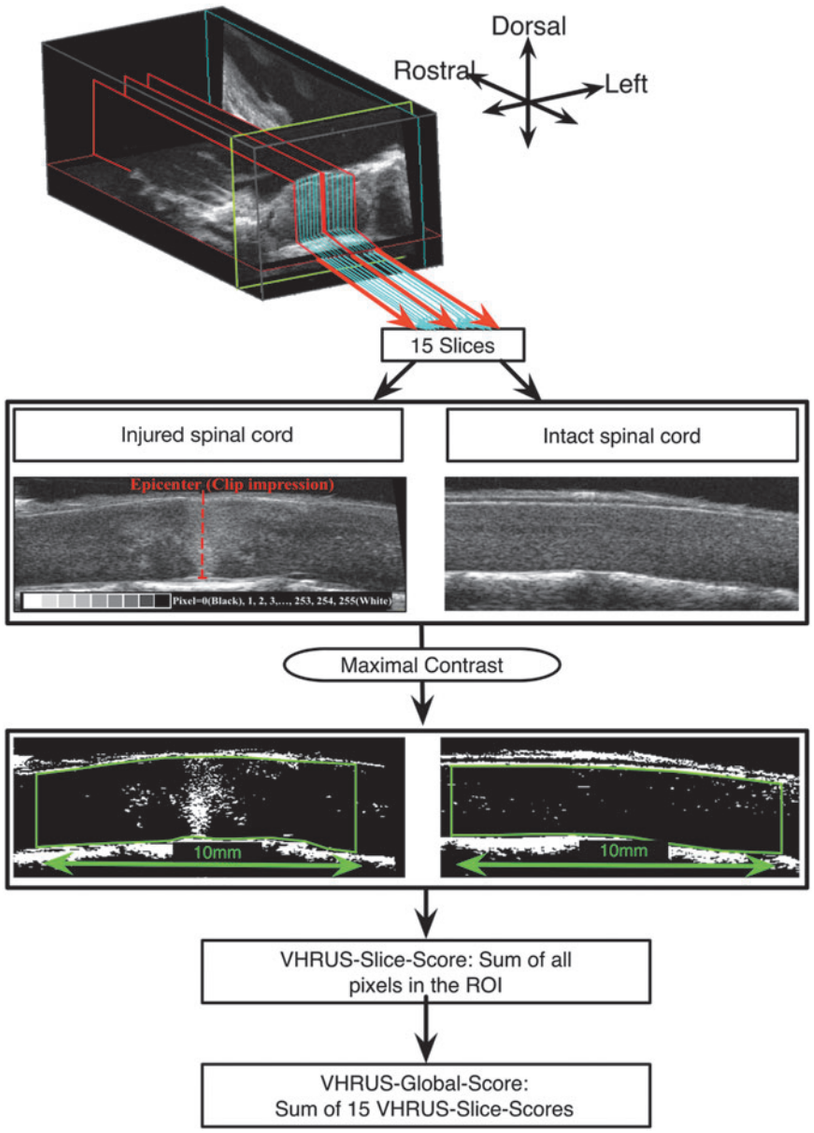

4C ▶

FIG. 3. Very high resolution ultrasound (VHRUS) quantification analysis methodology. The pixel brightness in contrast-enhanced images can readily and reliably identify the difference between ''injured'' and ''uninjured'' spinal cord tissue. ROI, region of interest.

Results

Eighty rats were used, six (7.5%) of which were excluded after VHRUS examination (performed immediately post-operatively) because of an accidental parenchymal hemorrhage induced by the laminectomy.

Part 1. Grayscale and vascular anatomy of the intact spinal cord

VHRUS examination in B-mode enabled the visualization of the gray scale anatomy of the spinal cord parenchyma and surrounding structures (Fig. 4). Examinations with power Doppler mode enabled the depiction of the intrinsic and extrinsic, arterial, and venous vasculature of the spinal cord (Fig. 5).

F4 ▶AU1 ▶

F5 ▶

Part 2. Characterization of post-SCI changes observed with VHRUS

Immediately after SCI, a hyperechoic lesion appeared in the parenchyma that extended during the next 24 h post-SCXI (Fig. 6). Power Doppler showed that sagittal vessels were no longer visible at the epicenter at 24 h post-SCI, and that the remaining blood vessels were pushed rostrally and caudally by the expanding hemorrhage.

◀F6

At 90 min post-SCI, the hyperechoic lesion observed on VHRUS was almost exclusively made up of extravasated red blood cells (i.e., PH) (Fig. 7), while at 24 h, it was a heterogeneous mix of erythrocytes, inflammatory cells, and debris. Fluorescence microscopy of extravasated Evans blue exhibited spatial patterns comparable to the VHRUS images (Fig. 8).

◀F7

◀F8

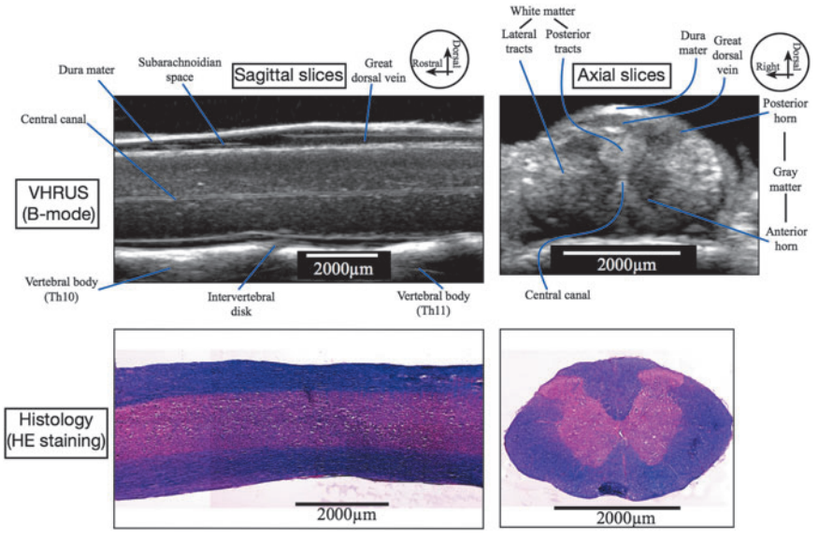

4C ▶

FIG. 4. Very high resolution ultrasound (VHRUS) structural anatomy of the intact spinal cord and correlation with corresponding histologic slices stained with hematoxylin and eosin (HE). With VHRUS examination in B-mode, the spinal cord parenchyma is slightly hyperechoic, and the white matter is slightly brighter than the gray matter. The central canal appears as a double hyperechoic line. The dura mater is also hyperechoic whereas the subarachnoid space is hypoechoic. The great dorsal vein is visible on the dorsal aspect of the spinal cord. The vertebral bodies and the intervertebral discs are also visible. Th10, 10th thoracic vertebr; Th11, 11th thoracic vertebra.

Part 3. Quantification of BSCB disruption with VHRUS

A significant correlation was found between the VHRUS-Global-Score and the amount of extravasated hemoglobin at 90 min post-SCI (Pearson $r=0.70$, $p=0.003$, $n=16$) and at 24 h post-SCI (Pearson $r=0.85$, $p<0.0001$, $n=22$) (Fig. 8). Similarly, at 24 h, a significant correlation was found between the VHRUS-Global-Score and the amount of extravasated Evans blue (Pearson $r=0.94$, $p<0.0001$, $n=22$) as well as between the latter and extravasated hemoglobin (Pearson $r=0.95$, $p<0.0001$, $n=22$). For measurements of the VHRUS-Global-Score, the Pearson correlation coefficients for intra- and interobserver reliability were both 0.99 ($p<0.0001$, $n=38$).

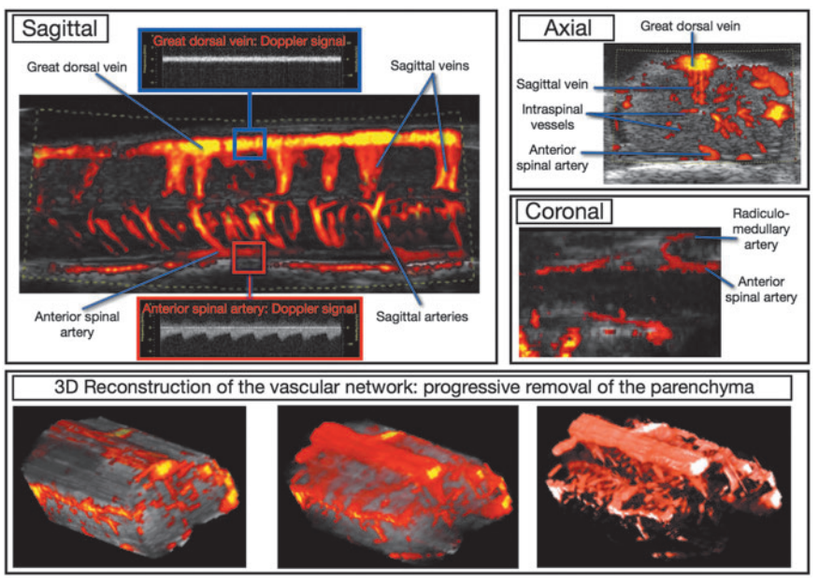

4C ▶

FIG. 5. Intrinsic and extrinsic spinal cord vasculature with very high resolution ultrasound in power Doppler mode. The anterior spinal artery is at the anterior part of the spinal cord splitting into several sagittal arteries. The great dorsal vein is at the dorsal aspect of the cord and drains the smaller sagittal veins. Doppler analysis confirmed the presence of pulsations into the anterior spinal artery while the great dorsal vein exhibited no pulsation. On coronal reconstruction, it is also possible to visualize the radiculo-medullary artery (originating from the segmental artery that arises from the aorta) along the neural roots and its anastomosis with the anterior spinal artery. This artery has a shape and location similar to the so-called Adamkiewicz artery described in humans. With three-dimensional (3D) Doppler acquisitions, it is possible to depict the complete vascular network by ''erasing'' the parenchyma.

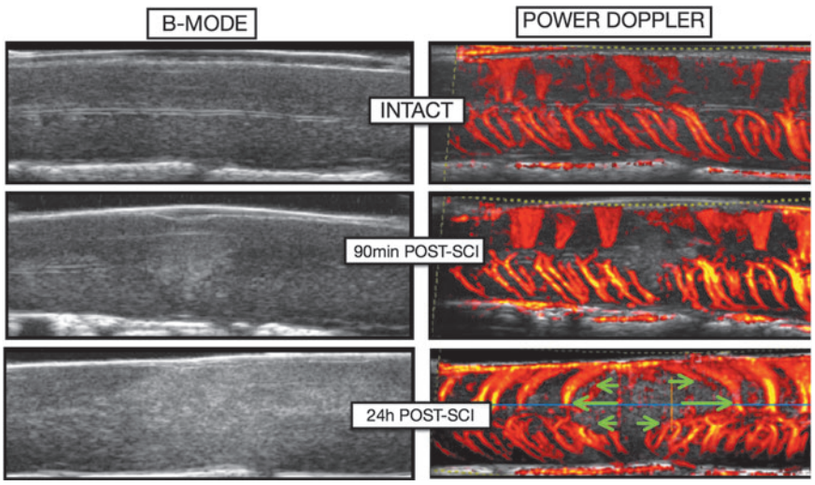

4C ▶

FIG. 6. Evolution of the parenchymal lesion on B-mode and the associated vascular network changes on power Doppler mode. Immediately after spinal cord injury (SCI), a hyperechoic lesion appears in the parenchyma and several sagittal vessels located at the epicenter are destroyed and no longer generate a detectable ultrasound signal. During the 24 h after SCI, the lesion expands rostrally and caudally, pushing away the remaining sagittal vessels (green arrows). The expansion of the secondary lesion progressively destroys perilesional areas that were spared initially (i.e. secondary injury).

V1 ▶ AU2 ▶ Time-lapse video acquisition (Video 1) showed that the PH progressively grew by two different mechanisms—namely, through persistent bleeding and the appearance of new foci of hemorrhage. The speed of growth (inset to Video 1) was maximal immediately after the injury and progressively slowed down, until it stabilized at about 90 min post-SCI at 19.3 ± 3% (standard deviation) of the value measured at 2 min post-SCI.

Discussion

In the present study, we have found for the first time that VHRUS is a powerful tool for depicting the structural and vascular anatomy of the spinal cord in rats. We also found that it can be repeated in the same animal, allowing for longitudinal *in vivo* studies. After SCI, a hyperechoic lesion appears in the parenchyma that precisely corresponds to the PH at the acute phase and depicts the injured areas where the BSCB is disrupted at 24 h post-SCI (i.e., the subacute phase). We have further demonstrated that VHRUS enables the quantification of hemorrhage (the amount of hemoglobin extravasated into the parenchyma) at 90 min and 24 h post-SCI, as well as the extent of vascular permeability (the amount of Evans blue bound to albumin extravasated) at 24 h post-SCI. Last, we have found that after SCI, two distinct mechanisms contribute to the extent of the PH—namely, the persistence of the intralesional bleeding and the subsequent appearance of numerous smaller secondary per-lesional foci of PH (confirmed by time-lapse video

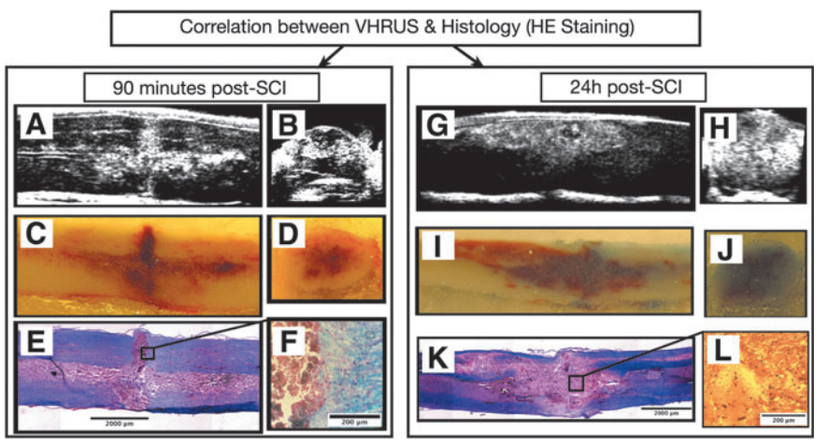

4C ▶

FIG. 7. Characterization of post-spinal cord injury (SCI) changes observed with very high resolution ultrasound (VHRUS) at the acute (90 min) and subacute (24 h) phases. (**A, G**) Sagittal VHRUS image. (**B, H**) Axial VHRUS image. (**C, I**) Embedded spinal cords during sagittal cryosectioning. (**D, J**) Embedded spinal cords during axial cryosectioning. (**E, F**) Histological slices. At 90 min post-SCI, an excellent correlation was found between the VHRUS images, the photographs of the embedded spinal cords, and the histological slices. The acute lesion observed on VHRUS was almost exclusively made up of extravasated red cells (i.e. parenchymal hemorrhage). At 24 h post-SCI, the parenchymal lesion observed with VHRUS is made up of a complex and heterogeneous mix of red blood cells, inflammatory cells, and tissue debris. HE, hematoxylin and eosin.

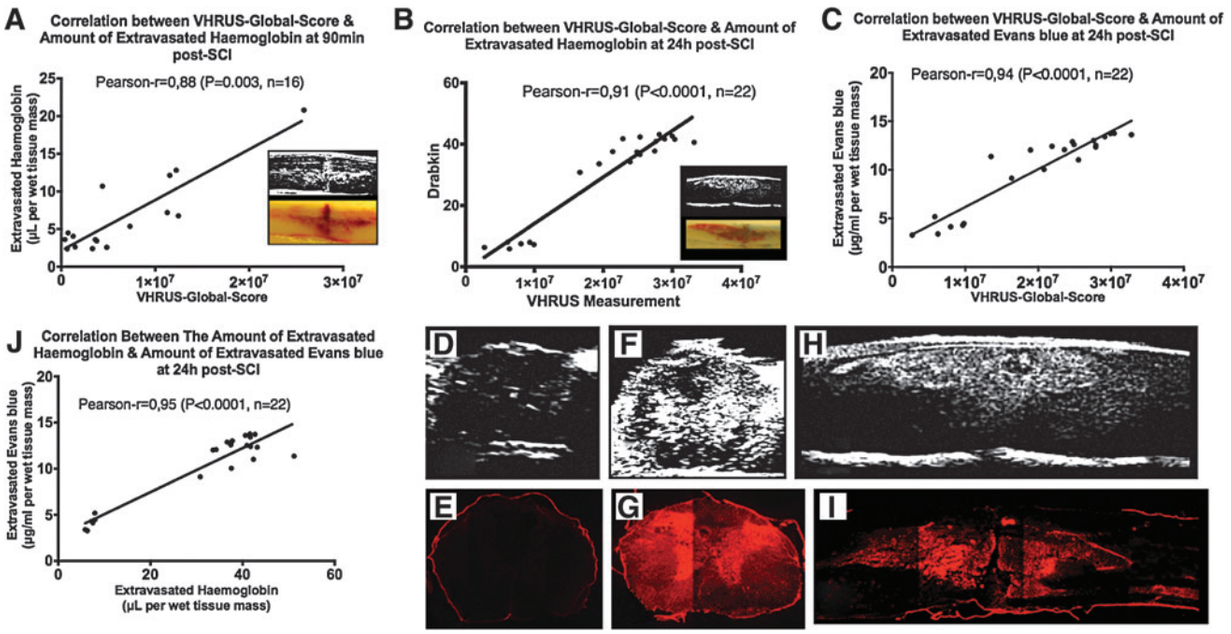

4C ▶

FIG. 8. Quantification of blood spinal cord barrier disruption with very high resolution ultrasound (VHRUS). (**A,B,C**) Correlations between VHRUS quantification and spectrophotometry assays at 90 min and 24 h post-spinal cord injury (SCI). (**D,E**) Axial slices of intact spinal cord obtained with VHRUS and fluorescent microscopy. (**F,G,H,I**) Axial and sagittal slices of injured spinal cords obtained with VHRUS and fluorescent microscopy of the Evans blue extravasation. (**J**) Correlation between the amounts of extravasated hemoglobin and Evans blue in the same animal. Significant statistical correlations were obtained between VHRUS quantification and spectrophotometry assays at 90 min and 24 h post-SCI. The spatial profile of Evans blue extravasation (red fluorescence) was strikingly similar to the VHRUS signal generated by the spinal cord lesion.

acquisition). We also concurrently highlighted an additional usefulness of VHRUS for monitoring and detecting the appearance of traumatic spinal cord PH caused by the laminectomy procedure and suggest that these go undetected in the majority of cases because there is no visually discernible bruising of the spinal cord in these rats.

These observations demonstrate the progressive secondary disruption of the BSCB after SCI, which is from the accumulation of cell debris, the generation of free radicals, calcium influx within the parenchyma, and the breakdown of tight junctions between endothelial cells.[31] This exacerbates the initial injury because the blood-borne species that enter the spinal cord parenchyma are toxic to neural cells and because the progressive and expanding vascular destruction leads to secondary perilesional ischemia.

Together, these data suggest that the effects of acute SCI treatments that target the vascular disruption could be accurately and repeatedly assessed by VHRUS imaging. This could have an important impact on clinical translational efforts, given that the lack of biomarkers to detect therapeutic effects is an important gap in the field that could be bridged by this technology.[32,33] In addition, given sufficient exposure of the lesioned spinal cord after decompressive laminectomy, peri- and intraoperative VHRUS has the potential to enhance the accuracy of prognosis of SCI by enabling a fast, safe, and accurate visualization of the severity and extent of the vascular lesion. It can also theoretically improve the accuracy of targeted stereotactic cell injections and minimize damage to spared tissue.

Other techniques described in the literature to visualize and/or quantify BSCB disruption involve either imaging or nonimaging techniques. Compared with nonimaging techniques such as quantifying extravasated Evans blue or hemoglobin, the main advantage of VHRUS is that it does not necessitate spinal cord isolation and consequently the animal can be kept alive, thereby allowing for repeated live-animal scans and reducing the number of animals needed.

The main imaging technique used to image *in-vivo* disruption of BSCB is MRI. Although MRI is less invasive because a laminectomy is not needed to image the spinal cord, it is much more expensive than VHRUS, requires dedicated facilities and staff, MRI equipment is neither compact nor mobile, is not compatible with ferromagnetic devices, and provides spatial resolution slightly inferior to VHRUS. Further, MRI does not allow real-time acquisition of the evolving PH because MRI acquisition takes much longer than VHRUS (the frame rate in B-mode is 25 images per sec in our study).

Histology and related techniques have better spatial resolution than VHRUS and allow for specific staining of molecules or cell populations that is not possible with conventional VHRUS (although recent developments in photoacoustic imaging do allow for *in vivo* real-time marking of systemically accessible tissues and cells).[34–36] Histology, however, requires harvest of the spinal cord, thereby precluding *in vivo* and real-time visualization of the spinal cord. Further, the isolation of the spinal cord releases the physiological tension that is present in the parenchyma and can therefore modify the morphology of the tissue, whereas the tissue fixation can provoke shrinkage of the tissue,[37–39] thereby limiting the findings of histological stereological studies. Many microhemorrhagic foci apparent on VHRUS were no longer detectable after histological processing of the spinal cord tissue. The ability of VHRUS to resolve anatomical structures 20–30 microns apart allows for extremely accurate

visualization of tissue and pathophysiological changes while preserving the exact *in vivo* morphology of tissues. In addition to the ability to perform 3D acquisitions, VHRUS is a valuable technique that can complement histology for stereological measurements.

In vivo microscopy is an imaging technique allowing for visualizing real-time cellular behavior.[36,40] It offers fascinating visualization at the cellular scale but, in comparison with VHRUS, it remains limited by at least two points. First, it requires animals genetically modified to express specific fluorescent proteins. Second, the depth of observation is limited to a few dozen of microns, which precludes deep observation of the spinal cord. In contrast, VHRUS allows visualization of the entire spinal cord and therefore represents a complementary imaging tool.

One of the classic limitations of US imaging is its operator dependency. US provides real-time bidimensional slices of the tissue acquired by the probe and when the probe is held by an operator, it poses two concerns—namely, the stability of the bidimensional image and the ability to find the exact same position in the same animal from one US examination to another. With the present protocol, we have solved this problem by using two strategies—the stabilization of the spine and the ability to perform 3D acquisitions.

Stabilization of the spine with the frame and clamping of the Th13 vertebra reduce movement of the spine and spinal cord associated with breathing, which otherwise interferes with US measurements. Spine stabilization is mandatory to obtain 3D acquisitions, power Doppler images, and time-lapse videos. Note that respiratory motions represent a common concern for many techniques for spinal cord imaging, for models of experimental SCI using an impactor, and for stereotactic intraspinal injections.[41] Solutions found in the literature are based on the use of a spinal clamp, increasing the depth of anesthesia, and on the use of respiratory machines to induce apnea.[42,43] Here, adequate stabilization of the whole spine was achieved by clamping Th13 and securing the incisor teeth to the nose cone.

The ability to perform 3D acquisitions was made possible by the use of a probe holder mounted on a motorized rail system. It allows for post-acquisition analysis of an infinite number of multiplanar reconstructions through the 3D file generated during imaging, each of which corresponds to a possible position of the probe when manually handled.

With conventional US probes available in clinical settings (12–15 MHz), the spatial resolution is around 100–200 microns per pixel while the VHRUS probe (44–50 MHz) offers a spatial resolution of 20–30 μm. Given that the rat spinal cord is about 3–4 mm[44] in diameter while the human spinal cord is about 1 cm,[45] it means that with VHRUS, it is possible to visualize a rat spinal cord as well as a human spinal cord with conventional US probes. Therefore, conclusions of experimental studies performed with VHRUS in rats are relevant to the clinic to improve the monitoring and prognosis of spinal cord injuries (e.g., intra- and perioperative US imaging during and immediately after decompressive laminectomy).

While this study was conducted in the lower thoracic spinal cord and focused on the acute and subacute phases of SCI, it is nonetheless applicable to injuries affecting other levels, even the cervical spinal cord, and imaging can be performed at chronic time points as well. Whatever spinal cord level is visualized, stabilization of the whole spine is performed identically as described in this study—namely, by stabilizing Th13 and the incisor teeth.

Conclusion

We demonstrate for the first time the application of VHRUS imaging to quantitatively assess the progression of vascular disruption after traumatic SCI. We anticipate that this technique will have an important impact on preclinical and clinical translational research efforts.

Acknowledgments

Dr. Marc Soubeyrand was supported by the SOFCOT (Société Française de Chirurgie Orthopédique et Traumatologique) and the APHP (Assistance Publique des Hôpitaux de Paris). Dr. Michael Fehlings is supported by the Halbert Chair in Neural Repair and Regeneration and receives funding from the Dezwirek Foundation.

Author contributions: Guarantor of integrity of entire study, all authors; study concepts/study design, experimental studies, and literature research, M.S., A.B., R.V.; manuscript drafting and revision, M.S., A.B., R.V., M.G.F., and Dr. Madeleine O'Higgins (Communications Specialist, Fehlings Team); approval of final version of submitted manuscript, all authors; data analysis, M.S, A.B., R.V., Y.S.C.; statistical analysis, M.S., M.G.F.

Author Disclosure Statement

No competing financial interests exist.

References

1. Kwon, B.K., Sekhon, L.H., and Fehlings, M.G. (2010). Emerging repair, regeneration, and translational research advances for spinal cord injury. Spine (Phila Pa 1976) 35, Suppl 21, S263–S270.
2. Fehlings, M.G., and Vawda, R. (2011). Cellular treatments for spinal cord injury: the time is right for clinical trials. Neurotherapeutics 8, 704–720.
3. Vawda, R., and Fehlings, M.G. (2013). Mesenchymal cells in the treatment of spinal cord injury: current & future perspectives. Curr. Stem Cell Res. Ther. 8, 25–38.
4. Lammertse, D.P. (2013). Clinical trials in spinal cord injury: lessons learned on the path to translation. The 2011 International Spinal Cord Society Sir Ludwig Guttmann Lecture. Spinal Cord 51, 2–9.
5. Mautes, A.E., Weinzierl, M.R., Donovan, F., and Noble, L.J. (2000). Vascular events after spinal cord injury: contribution to secondary pathogenesis. Phys. Ther. 80, 673–687.
6. Tator, C.H., and Fehlings, M.G. (1991). Review of the secondary injury theory of acute spinal cord trauma with emphasis on vascular mechanisms. J. Neurosurg. 75, 15–26.
7. Noble, L.J., and Wrathall, J.R. (1989). Distribution and time course of protein extravasation in the rat spinal cord after contusive injury. Brain Res. 482, 57–66.
8. Popovich, P.G., Horner, P.J., Mullin, B.B., and Stokes, B.T. (1996). A quantitative spatial analysis of the blood-spinal cord barrier. I. Permeability changes after experimental spinal contusion injury. Exp. Neurol. 142, 258–275.
9. Figley S.A., Khosravi R., Legasto J.M., Tseng Y.F., and Fehlings M.G. (2014). Characterization of vascular disruption and blood-spinal cord barrier permeability following traumatic spinal cord injury. J. Neurotrauma 31, 541–552.
10. Yu, F., Kamada, H., Niizuma, K., Endo, H., and Chan, P.H. (2008). Induction of mmp-9 expression and endothelial injury by oxidative stress after spinal cord injury. J Neurotrauma 25, 184–195.
11. Austin, J.W., Afshar, M., and Fehlings, M.G. (2012). The relationship between localized subarachnoid inflammation and parenchymal pathophysiology after spinal cord injury. J. Neurotrauma 29, 1838–1849.
12. Cohen, D.M., Patel, C.B., Ahobila-Vajjula, P., Sundberg, L.M., Chacko, T., Liu, S.J., and Narayana, P.A. (2009). Blood-spinal cord barrier permeability in experimental spinal cord injury: dynamic contrast-enhanced MRI. NMR Biomed. 22, 332–341.
13. Maikos, J.T., and Shreiber, D.I. (2007). Immediate damage to the blood-spinal cord barrier due to mechanical trauma. J. Neurotrauma 24, 492–507.
14. Noble, L.J., and Wrathall, J.R. (1989). Correlative analyses of lesion development and functional status after graded spinal cord contusive injuries in the rat. Exp. Neurol. 103, 34–40.

15. Babyn, P.S., Chuang, S.H., Daneman, A., and Davidson, G.S. (1988). Sonographic evaluation of spinal cord birth trauma with pathologic correlation. AJR. Am J Roentgenol 151, 763–766.
16. Chadduck, W.M., and Flanigan, S. (1985). Intraoperative ultrasound for spinal lesions. Neurosurgery 16, 477–483.
17. de Vries, E., Robben, S.G., and van den Anker, J.N. (1995). Radiologic imaging of severe cervical spinal cord birth trauma. Eur. J. Pediatr. 154, 230–232.
18. Finn-Bodner, S.T., Hudson, J.A., Coates, J.R., Sorjonen, D.C., Simpson, S.T., Cox, N.R., Wright, J.C., Garrett, P.D., Steiss, J.E., Vaughn, D.M., Miller, S.C., and Brown, S.A. (1995). Ultrasonographic anatomy of the normal canine spinal cord and correlation with histopathology after induced spinal cord trauma. Vet. Radiol. Ultrasound 39–48.
19. Huang, L., Lin, X., Tang, Y., Yang, R., Li, A.H., Ye, J.C., Chen, K., Wang, P., and Shen, H.Y. (2013). Quantitative assessment of spinal cord perfusion by using contrast-enhanced ultrasound in a porcine model with acute spinal cord contusion. Spinal Cord 51, 196–201.
20. Jones, C.F., Cripton, P.A., and Kwon, B.K. (2012). Gross morphological changes of the spinal cord immediately after surgical decompression in a large animal model of traumatic spinal cord injury. Spine (Phila Pa 1976) 37, E890–E899.
21. Soubeyrand, M., Laemmel, E., Dubory, A., Vicaut, E., Court, C., and Duranteau, J. (2012). Real-time and spatial quantification using contrast-enhanced ultrasonography of spinal cord perfusion during experimental spinal cord injury. Spine (Phila Pa 1976) 37, E1376–E1382.
22. Moran, C.M., Pye, S.D., Ellis, W., Janeczko, A., Morris, K.D., McNeilly, A.S., and Fraser, H.M. (2011). A comparison of the imaging performance of high resolution ultrasound scanners for preclinical imaging. Ultrasound Med. Biol. 37, 493–501.
23. Pistner, A., Belmonte, S., Coulthard, T., and Blaxall, B. (2010). Murine echocardiography and ultrasound imaging. J. Vis. Exp. 42.
24. Rivlin, A.S., and Tator, C.H. (1978). Effect of duration of acute spinal cord compression in a new acute cord injury model in the rat. Surg. Neurol. 10, 38–43.
25. Fehlings, M.G., and Tator, C.H. (1995). The relationships among the severity of spinal cord injury, residual neurological function, axon counts, and counts of retrogradely labeled neurons after experimental spinal cord injury. Exp. Neurol. 132, 220–228.
26. Manaenko, A., Chen, H., Kammer, J., Zhang, J.H., and Tang, J. (2011). Comparison Evans Blue injection routes: Intravenous versus intraperitoneal, for measurement of blood-brain barrier in a mice hemorrhage model. J. Neurosci. Methods 195, 206–210.
27. Tian, D.S., Liu, J.L., Xie, M.J., Zhan, Y., Qu, W.S., Yu, Z.Y., Tang, Z.P., Pan, D.J. and Wang, W. (2009). Tamoxifen attenuates inflammatory-mediated damage and improves functional outcome after spinal cord injury in rats. J. Neurochem. 109, 1658–1667.
28. Chen, X., Lan, X., Roche, I., Liu, R., and Geiger, J.D. (2008). Caffeine protects against MPTP-induced blood-brain barrier dysfunction in mouse striatum. J. Neurochem. 107, 1147–1157.
29. Drabkin, D.L. (1965). The Molecular weight of haemoglobin, its iron and nitrogen content and optical properties—their relevance in the problem of a reference standard for haemoglobin measurement. Bibl. Haematol. 21, 33–42.
30. Moore, G.L., Ledford, M.E., and Merydith, A. (1981). A micromodification of the Drabkin hemoglobin assay for measuring plasma hemoglobin in the range of 5 to 2000 mg/dl. Biochem. Med. 26, 167–173.
31. Oudega, M. (2012). Molecular and cellular mechanisms underlying the role of blood vessels in spinal cord injury and repair. Cell Tissue Res 349, 269–288.
32. Fan, Z.K., Lv, G., Wang, Y.F., Li, G., Yu, D.S., Wang, Y.S., Zhang, Y.Q., Mei, X.F. and Cao, Y. (2013). The protective effect of salvianolic acid B on blood-spinal cord barrier after compression spinal cord injury in rats. J. Mol. Neurosci. 51, 986–993.
33. Cadotte D.W., and Fehlings M.G. (2013). Spinal cord injury: visualizing plasticity and repair in the injured CNS. Nat. Rev. Neurol. 9, 546–547.
34. Jokerst, J.V., Thangaraj, M., Kempen, P.J., Sinclair, R., and Gambhir, S.S. (2012). Photoacoustic imaging of mesenchymal stem cells in living mice via silica-coated gold nanorods. ACS Nano 6, 5920–5930.
35. Wang, L.V. (2009). Multiscale photoacoustic microscopy and computed tomography. Nat. Photonics 3, 503–509.
36. Lichtman, J.W., and Fraser, S.E. (2001). The neuronal naturalist: watching neurons in their native habitat. Nat. Neurosci. 4 Suppl, 1215–1220.
37. West, M.J. (2013). Tissue shrinkage and stereological studies. Cold Spring Harb. Protoc. 2013.
38. Carlo, C.N., and Stevens, C.F. (2011). Analysis of differential shrinkage in frozen brain sections and its implications for the use of guard zones in stereology. J. Comp. Neurol. 519, 2803–2810.
39. Diemer, N.H. (1982). Quantitative morphological studies of neuropathological changes. Part 1. Crit. Rev. Toxicol. 10, 215–263.
40. Misgeld, T., and Kerschensteiner, M. (2006). In vivo imaging of the diseased nervous system. Nat. Rev. Neurosci. 7, 449–463.
41. Guest, J., Benavides, F., Padgett, K., Mendez, E., and Tovar, D. (2011). Technical aspects of spinal cord injections for cell transplantation. Clinical and translational considerations. Brain Res. Bull. 84, 267–279.
42. Davalos, D., Lee, J.K., Smith, W.B., Brinkman, B., Ellisman, M.H., Zheng, B., and Akassoglou, K. (2008). Stable in vivo imaging of densely populated glia, axons and blood vessels in the mouse spinal cord using two-photon microscopy. J. Neurosci. Methods 169, 1–7.
43. Romanelli, E., Sorbara, C.D., Nikic, I., Dagkalis, A., Misgeld, T., and Kerschensteiner, M. (2013). Cellular, subcellular and functional in vivo labeling of the spinal cord using vital dyes. Nat. Protoc. 8, 481–490.
44. Watson, C., Paxinos, G., and Kayalioglu, G. (2008) *The Spinal Cord* (A Christopher and Dana Reeve Foundation Text and Atlas). Elsevier Science: New York.
45. Ko, H.Y., Park, J.H., Shin, Y.B., and Baek, S.Y. (2004). Gross quantitative measurements of spinal cord segments in human. Spinal Cord 42, 35–40.

Address correspondence to:
Michael G. Fehlings, MD, PhD
Division of Genetics and Development
Toronto Western Research Institute
Krembil Neuroscience Program
University Health Network
Krembil Discovery Tower
60, Leonard Street
Toronto, ON M5T 2S8
Canada

E-mail: michael.Fehlings@uhn.ca

VIDEO 1. Time-lapse video of the evolving parenchymal hemorrhage during the first 90 min after SCI. First, some foci of hemorrhage that were present immediately after the clip injury continued to extend. Second, some areas free of hemorrhage exhibit very sudden (from one frame to the next one) appearance of new foci of hemorrhage. Constant visualization of the central canal confirms that the slice was always obtained on the same spot. Inset: The extent of the parenchymal hemorrhage has been calculated by repeating measurement of the VHRUS-Slice-Score and the inset graph shows the data obtained in six animals. ◀AU2

AUTHOR QUERY FOR NEU-2013-3319-VER9-SOUBEYRAND_1P

AU1: Figure 3 has not been cited in the text. Please cite it in an appropriate place ahead of Figure 4 so that figure numbers are cited in numerical order in the text.

AU2: We note mention of Video 1 in the text and a caption, but we do not see a video. Is it to be available online as a supplementary item? Please advise.

AU3: Do you mean: spectrophotometry? If so, please correct in flowchart.